

Knowledge Distillation from Language-Oriented to Emergent Communication for Multi-Agent Remote Control

Yongjun Kim, *Sejin Seo, †Jihong Park, ‡Mehdi Bennis, *Seong-Lyun Kim, and Junil Choi

Abstract—In this work, we compare emergent communication (EC) built upon multi-agent deep reinforcement learning (MADRL) and language-oriented semantic communication (LSC) empowered by a pre-trained large language model (LLM) using human language. In a multi-agent remote navigation task, with multimodal input data comprising location and channel maps, it is shown that EC incurs high training cost and struggles when using multimodal data, whereas LSC yields high inference computing cost due to the LLM’s large size. To address their respective bottlenecks, we propose a novel framework of language-guided EC (LEC) by guiding the EC training using LSC via knowledge distillation (KD). Simulations corroborate that LEC achieves faster travel time while avoiding areas with poor channel conditions, as well as speeding up the MADRL training convergence by up to 61.8% compared to EC.

Index Terms—Semantic communication (SC), language-oriented SC, emergent communication, large language model (LLM), knowledge distillation.

I. INTRODUCTION

Semantic communication (SC) is an emerging research paradigm aimed at designing efficient and effective communication for specific tasks [1]. Unlike traditional communication systems centered on the accurate delivery of raw data, SC focuses on conveying effective meanings or intention for given tasks, also referred to as semantic representations (SRs). Machine learning (ML) plays a crucial role in extracting these SRs from complex raw data, and recent works in this area can be broadly categorized into bottom-up and top-down approaches. The bottom-up approach allows SRs to naturally emerge from multi-way task-specific interactions. A prominent example is deep joint source and channel coding (DeepJSCC) for data reconstruction or other inference tasks [2], wherein SRs emerge as latent variables within an encoder-decoder architected neural network (NN). Another example is emergent communication (EC) for multi-agent control tasks [3], [4]. In EC, NN-structured agents exchange their hidden-layer activations by means of a multi-agent deep reinforcement learning (MADRL) framework. These activations, which are

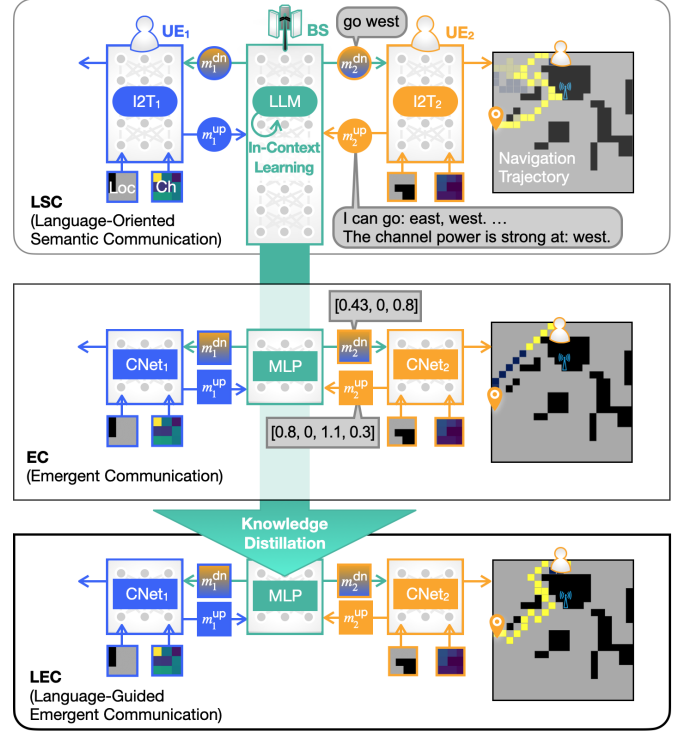


Fig. 1: A schematic illustration of: LSC (top), EC (middle), and LEC (bottom).

initially random values, become meaningful SRs for inter-agent coordination after training completes. While provisioning fast inference speed after training, the MADRL training process is costly and prone to bias, particularly when dealing with multi-modal data.

Conversely, the top-down approach first imposes a pre-defined structure on SRs, and transforms raw data into such structured SRs. Language-oriented SC (LSC) falls into this category, which considers natural language as a pre-defined structure to leverage the capabilities of large language models (LLMs) built upon natural language [5]–[9]. Precisely, LSC first utilizes pre-trained multi-modal generative models to convert raw data samples into text embeddings, such as the BLIP model for image-to-text conversion [6]. These text-based SRs instruct a pre-trained LLM to carry out various tasks including compression [7], context reasoning [8], and control decision-making [9]. While LLMs consume a large computing cost per inference, they can instantly adapt to new

Y. Kim and J. Choi are with the School of Electrical Engineering, KAIST, Daejeon 34141, Korea (email: {yongjunkim, junil}@kaist.ac.kr).

†J. Park is with the School of Information Technology, Deakin University, VIC 3218, Australia (email: jihong.park@deakin.edu.au).

‡M. Bennis is with the Centre for Wireless Communications, University of Oulu, Oulu 90570, Finland (email: mehdi.bennis@oulu.fi).

*S. Seo and S.-L. Kim are with the School of Electrical & Electronic Engineering, Yonsei University, Seoul 03722, Korea (email: {sjseo, slkim}@ramo.yonsei.ac.kr).

J. Choi and J. Park are corresponding authors.

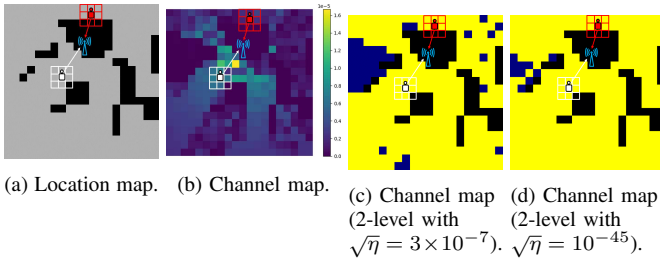


Fig. 2: Global map wherein each UE observes within 3×3 FoV.

tasks by providing demonstration with examples. This unique capability of LLMs is called in-context learning, which bears a significant advantage over EC that requires MADRL re-training for such adaptation.

To harness the merits of both approaches, we propose a novel framework of language-guided EC (LEC) by integrating LSC into EC. As illustrated in Fig. 1, LEC employs an in-context learned LSC as a teacher to guide an EC as its student via knowledge distillation (KD), an ML technique to synchronize outputs for common inputs [10]. To demonstrate the feasibility of LEC, we consider a multi-agent remote control and navigation task, wherein agents aim to reach their target destinations while avoiding poor channel conditions. During the task, each agent perceives its local location and channel maps while exchanging SRs with a base station (BS).

We verify that EC is biased towards location maps, leading to frequent encounters with poor channels. LSC avoids poor channels, but the trajectories vary significantly over episodes. This variability is presumably due to the LLM's enforcing inference despite uncertainty, also known as LLM hallucinations, and resultant error propagation in the LLM's memory or within its context window. To address this, we develop a method to refine and select the top- L LSC trajectories for teacher knowledge, and a modified KD method to reflect this. Simulations show that LEC achieves 61.8% less average training steps to convergence compared to EC. Furthermore, LEC achieves low computing costs during both training and inference, thanks to in-context learning of LSC and training convergence acceleration of KD in EC.

II. SYSTEM MODEL

A. Network and Channel Model

The network under study consists of a single BS associated with a set \mathcal{J} of user equipments (UEs). In a square grid $\mathcal{M} \subset \mathbb{R}^2$, the location $\mathbf{z}_{bs} \in \mathcal{M}$ of the BS is fixed at the top of a building, as shown by the global location map in Fig. 2(a) where the area $\mathcal{M}_b \subset \mathcal{M}$ of buildings is colored in black. At a time step t , the j -th UE is located at $\mathbf{z}_j^t \in \mathcal{M} \setminus \mathcal{M}_b$. To coordinate and control multiple agents, the BS broadcast a downlink (DL) message $m^{\text{dn},t}$ with power $P_j^{\text{dn},t}$ to all UEs. Assuming sufficiently large $P_j^{\text{dn},t}$, we consider that DL communication is error-free, and the received DL message at every UE is $m^{\text{dn},t}$.

By contrast, each UE has a limited transmit power $P_j^{\text{up},t}$, leading to erroneous uplink (UL) message reception under

noisy channels. Precisely, to report local information to the BS, the j -th UE transmits an UL message $m_j^{\text{up},t}$, and the received UL message at the BS is:

$$\tilde{m}_j^{\text{up},t} = h_{\mathbf{z}_j^t} \sqrt{P_j^{\text{up},t}} m_j^{\text{up},t} + n, \quad (1)$$

where $h_{\mathbf{z}_j^t}$ is the UL wireless channel from \mathbf{z}_j^t to \mathbf{z}_{bs} , and $n \sim \mathcal{CN}(0, \sigma^2)$. According to (1), the received UL signal-to-noise ratio (SNR) is $P_j^{\text{up},t} |h_{\mathbf{z}_j^t}|^2 / \sigma^2$. Assuming time division duplexing (TDD), the UL channel gain $|h_{\mathbf{z}_j^t}|^2$ is reciprocal with its DL channel gain, which is visualized by the global channel map in Fig. 2(b). To maintain a constant target received SNR P_r / σ^2 at the BS, the UE applies channel inversion power control such that the transmit power $P_j^{\text{up},t}$ is set as $P_r / |h_{\mathbf{z}_j^t}|^2$.

B. Multi-Agent Remote Navigation Task

The j -th UE is initially located at \mathbf{z}_j^0 , and moves to reach a pre-determined destination $\hat{\mathbf{z}}_j \in \mathcal{M} \setminus \mathcal{M}_b$. Each UE aims to achieve two objectives: 1) minimizing the number of T_j time stamps required to reach its destination, such that $\mathbf{z}_j^{T_j} = \hat{\mathbf{z}}_j$ for all $j \in \mathcal{J}$; while 2) avoiding the locations in $\mathcal{M}_w \subset \mathcal{M} \setminus \mathcal{M}_b$ associated with weak channels. Given the channel inversion power control, the weak channel condition is defined as $|h_{\mathbf{z}_j^t}|^2 < \eta$ with $\eta := P_r / P_{\text{th}}$ in which the UE transmit power exceeds a target power budget P_{th} , i.e., $P_j^{\text{up},t} > P_{\text{th}}$.

To achieve this goal, at each time t , the j -th UE observes its local location map L_j^t and local channel map C_j^t within its 3×3 field of view (FoV), as depicted in Fig. 2. To report this multimodal data $\{L_j^t, C_j^t\}$, the UE transmits an UL message $m_j^{\text{up},t}$ to the BS. The BS receives the UL message collection $\tilde{m}^{\text{up},t} = \{\tilde{m}_1^{\text{up},t}, \tilde{m}_2^{\text{up},t}, \dots, \tilde{m}_{|\mathcal{J}|}^{\text{up},t}\}$ from all UEs, and thereby generates a DL message $m^{\text{dn},t}$ that is broadcasted to all UEs. Based on the received $m^{\text{dn},t}$, the j -th UE takes an action a_j^t from an action space $\mathcal{A} := \{(-v, -v), (-v, 0), (-v, v), (0, -v), (0, v), (v, -v), (v, 0), (v, v)\}$, where v is the unit traveling distance in one time step. There are invalid actions that result in inter-UE collision, out-of-area, and building blockage, i.e., $\mathbf{z}_j^{t+1} = \mathbf{z}_i^{t+1}$ with $i \neq j$, $\mathbf{z}_j^{t+1} \notin \mathcal{M}$, and $\mathbf{z}_j^{t+1} \in \mathcal{M}_b$, respectively. For such invalid actions, the UE remains the previous position, i.e., $\mathbf{z}_j^{t+1} = \mathbf{z}_j^t$.

III. EMERGENT COMMUNICATION VERSUS LANGUAGE-ORIENTED SEMANTIC COMMUNICATION

In this section, we introduce EC and LSC. Throughout the paper, EC exchanges modulated symbols optimized during MADRL training, while LSC exchanges natural language messages digitally encoded using 8-bits ASCII code and modulated by 16QAM.

A. Emergent Communication

The j -th UE has at time slot t has an input state $s_j^t = \{s_{j_1}^t, s_{j_2}^t\}$, where $s_{j_1}^t := \{L_j^t, C_j^t\}$ involves a local location map and a local channel map while $s_{j_2}^t$ is the image of the UE's movement trajectory until t . For EC framework depicted in the middle of Fig. 1, a model $G_j(\cdot)$ named CNet generates

the current action a_j^t , subsequent hidden state of a recurrent neural network (RNN) h_j^{t+1} , and the UL message $m_j^{\text{up},t}$ from the current state s_j^t and the last received DL message $m_j^{\text{dn},t}$, i.e., $(a_j^t, h_j^{t+1}, m_j^{\text{up},t}) = G_j(s_j^t, h_j^t, m_j^{\text{dn},t})$. The BS employs multilayer perceptron (MLP) $G_{\text{bs}}(\cdot)$ to generate DL messages from the UL messages as $m^{\text{dn},t+1} = G_{\text{bs}}(\tilde{m}^{\text{up},t})$. The set of the parameters of $G_{\text{bs}}(\cdot)$ and $G_j(\cdot)$ denoted as $\theta := \{\theta_{\text{bs}}, \cup_{j=1}^{|\mathcal{J}|} \theta_j\}$ is optimized by minimizing the Deep-Q learning loss function as (4). Here, $Q(\cdot)$ and $Q'(\cdot)$ represent the current and target Q networks, respectively. The state-action pairs (s_j^t, a_j^t) and (s_j^t, a_j^t) denote the inputs to the respective Q-networks. The reward function r_j^t is defined as:

$$r_j^t = \begin{cases} 10, & \text{if } \mathbf{z}_j^t = \hat{\mathbf{z}}_j \\ -0.1, & \text{if } \mathbf{z}_j^{t+1} = \mathbf{z}_j^t \\ -0.1, & \text{if } |h_{\mathbf{z}_j^t}|^2 \leq \eta \\ -0.01 & \text{if } \mathbf{z}_j^t \neq \hat{\mathbf{z}}_j. \end{cases} \quad (2)$$

Each reward value corresponds to (i) reaching the target, (ii) invalid action, (iii) exceeding the power budget, and (iv) time consumption, respectively. Based on the acquired θ_{EC}^* , the policy is determined by

$$(\text{EC}) \quad a_j^t = \arg \max_a p(a | s_j^t, h_j^t, \tilde{m}_j^{\text{dn},t}; \theta_{\text{EC}}^*), \quad (3)$$

where θ_{EC}^* denotes the trained model parameters given in (4).

B. Language-Oriented Semantic Communication

In LSC, as illustrated in Fig. 1, each UE employs an image-to-text (I2T) generative model $G_{\text{Gen},j}(\cdot)$ to transform $s_{j_1}^t$ into a natural language message $m_{j_1}^{\text{up},t} = G_{\text{Gen},j}(s_{j_1}^t)$. The message $m_{j_1}^{\text{up},t}$ is complemented by additional textual information $m_{j_2}^{\text{up},t}$ that provides direction guidance towards the destination $\hat{\mathbf{z}}_j$ by reporting the remaining taxicab distance to the destination. Consequently, the UL message is given by $m_j^{\text{up},t} = \{m_{j_1}^{\text{up},t}, m_{j_2}^{\text{up},t}\}$. The BS aggregates the received UL messages from all UEs, i.e., $\tilde{m}^{\text{up},t} = \{\tilde{m}_1^{\text{up},t}, \tilde{m}_2^{\text{up},t}, \dots, \tilde{m}_{|\mathcal{J}|}^{\text{up},t}\}$, and produces the DL message $m^{\text{dn},t} = G_{\text{LLM}}(\tilde{m}^{\text{up},t}) = \{m^{\text{res},t}, m_1^{\text{a},t}, m_2^{\text{a},t}, \dots, m_{|\mathcal{J}|}^{\text{a},t}\}$ using an LLM $G_{\text{LLM}}(\cdot)$. The DL messages involve the message $m_j^{\text{a},t}$ to instruct an action to the j -th UE, as well as the message $m^{\text{res},t}$ explaining the rationale behind the LLM's action decisions.

The current LLM often struggles when dealing with continuous values [5]–[9]. To detour this, we quantize the amplitudes of the original global channel map in Fig. 2b into two levels, before inputting $s_{j_1}^t$ into $G_{\text{Gen},j}(\cdot)$ and $G_j(\cdot)$. Such

UE 1 : "I can go to : south, east, southeast. From the location (x=0, y=0) aiming for (x=9, y=9), the direction that goes closest to the goal is southeast. Other directions like northeast, east, southwest and south will also get me closer. The channel power is strong at south, east, southeast."
 UE 2 : "I can go to : west, southwest, south, east, southeast. From the location (x=0, y=0) aiming for (x=10, y=0), the direction that goes closest to the goal is southwest. Other directions like northwest, west, south and southeast will also get me closer. The channel power is strong at west, south, east, southeast. The channel power is weak at southwest, so the communication service is unstable."
 Question : Which direction should UE 1 and UE 2 go?

(a) UL messages $\tilde{m}^{\text{up},t}$ at SNR = 20dB.

UE 1 : "I go to : south, east, southeast. From the location (x=0, y=0) aiming for (x=9, y=9), the direction that goes closest to the goal is southeast. Other directions like northeast, east, southwest and south will also get me closer. The channel power is strong at south, east, southeast."
 UE 2 : "I go to : west, southwest, south, east, southeast. From the location (x=0, y=0) aiming for (x=10, y=0), the direction that goes closest to the goal is southwest. Other directions like northwest, west, south and southeast will also get me closer. The channel power is strong at west, south, east, southeast. The channel power is weak at southwest, so the communication service is unstable."

(b) UL messages $\tilde{m}^{\text{up},t}$ at SNR = 15dB.

Explanation : UE 1 should choose "southeast" as it brings them closer to the goal and has strong channel power. UE 2 should choose "west" as it brings them closer to the goal, avoiding "southwest" due to weak channel power.
 UE 1 : southeast
 UE 2 : west

Explanation : UE 1 should choose southeast as it brings them closer to the goal and has strong channel power, while avoiding weak channels. UE 2 should choose southwest as it brings them closer to the goal, although southeast is a closer direction. UE 2 should avoid weak channels as much as possible.
 UE 1 : southeast
 UE 2 : southwest

Explanation : What is the goal of the task? What are the constraints of the task? What are the wireless channel strengths?
 UE 1 : none
 UE 2 : none

(c) DL message $m^{\text{dn},t}$ at SNR = 20dB, $K = 2$. (d) DL message $m^{\text{dn},t}$ at SNR = 15dB, $K = 2$. (e) DL message $m^{\text{dn},t}$ at SNR = 15dB, $K = 0$.

Fig. 3: Example prompts of LSC.

quantization aligns with the goal of our task, avoiding weak channel conditions associated with the areas \mathcal{M}_w , as described in Sec. II-B. As visualized by the quantized global channel maps in Fig. 2c and 2d, dark blue regions represent \mathcal{M}_w , which decrease with the transmit power budget P_{th} .

In EC, task-specific knowledge is learned and stored in θ_{EC}^* , and therefore actions in (3) are determined by only providing current observations and received messages. In LSC, by contrast, the pre-trained LLM θ_{LLM} is general knowledge, which becomes task-specific by additionally providing task-related text prompts. Such additional prompts include: the BS's history of previously received UL messages and produced DL messages $m_{t-1}^{\text{bs}} = \cup_{u=1}^{t-1} \{\tilde{m}^{\text{up},u}, m^{\text{dn},u}\}$, a meta instruction x' outlining task outlining task guidelines and the role of the BS, and K -pair examples $c_K = \{(i_1, o_1), (i_2, o_2), \dots, (i_K, o_K)\}$. Consequently, the action a_j^t in LSC are determined as follows:

$$(\text{LSC}) \quad a_j^t = F\left(\arg \max_m p(m | \tilde{m}^{\text{up},t}, m_{t-1}^{\text{bs}}, c_K; \theta_{\text{LLM}})\right), \quad (5)$$

Here, the function $F(\cdot)$ converts a text message $m_i \in \mathcal{A}_m$ into an action $a_i \in \mathcal{A}$, i.e., $a_i = F(m_i)$, where $\mathcal{A}_m := \{\text{'northwest'}, \text{'north'}, \text{'northeast'}, \text{'west'}, \text{'east'}, \text{'southwest'}, \text{'south'}, \text{'southeast'}\}$.

$$\theta_{\text{EC}}^* = \arg \min_{\theta} \left\{ \mathbb{E} \left[\sum_{j,t} \left[\{r_j^t + \gamma \max_{a_j^t} Q'(s_j^t, a_j^t | \theta) - Q(s_j^t, a_j^t | \theta)\}^2 \right] \right] \right\} \quad (4)$$

$$\theta_{\text{LEC}}^* = \arg \min_{\theta} \left\{ \mathbb{E} \left[\sum_{j,t} \left[\{\tilde{r}_j^t + \gamma \max_{a_j^t} Q'(s_j^t, a_j^t | \theta) - Q(s_j^t, a_j^t | \theta)\}^2 + \lambda \mathcal{L}_{\text{KLD}} \right] \right] \right\} \quad (12)$$

TABLE I: Computing cost comparison among EC, LSC, and LEC (using [12] for UEs in LSC and ‘calflops’ [13] library for the rest).

	FLOPs		Number of Parameters	
	UE	BS	UE	BS
LSC	22.5G	17.57T	109M	68.71B
EC	25.63M	34.05K	278.31K	2.24K
LEC	25.63M	34.05K	278.31K	2.24K

In (5), c_K facilitates in-context learning, i.e., learning via demonstration with examples, which can be explained through the lens of a recent theory on LLM latent spaces [11]. Precisely, consider an ϵ -ambiguity message x , defined as a message for which $p(\phi|x) \geq 1 - \epsilon(x)$. The term $\epsilon(x) \in [0, 1]$ represents the degree of ambiguity, and $p(\phi|x)$ is the possibility of inferring the original intention ϕ from x . According to Proposition 3 in [11], the difference between LLM’s prediction probability $p(m^{\text{dn},t}|\tilde{m}^{\text{up},t}, c_K, i_{K+1})$ using K -shot in-context learning samples c_K and the true conditional probability $q(m^{\text{dn},t}|i_{K+1}, \phi_{c_K})$ with an unknown common intention ϕ_{c_K} is bounded as follows:

$$|p(m^{\text{dn},t}|\tilde{m}^{\text{up},t}, c_K, i_{K+1}) - q(m^{\text{dn},t}|i_{K+1}, \phi_{c_K})| \leq \epsilon(\tilde{m}^{\text{up},t})\epsilon(i_{K+1}) \prod_{k=1}^K \epsilon(i_k, o_k). \quad (6)$$

Since the rightmost term decreases with K following a power law, only a few K examples can significantly enhance the LLM’s prediction accuracy through in-context learning.

Fig. 3 displays examples of the received UL messages $\tilde{m}^{\text{up},t}$ and the produced DL messages $m^{\text{dn},t}$ at the BS. Low SNR distorts the UL messages as observed by comparing Fig. 3a and 3b. Due to the UL message distortion, the DL message in Fig. 3d yields wrong actions $m_1^{a,t}$, and $m_2^{a,t}$ and inappropriate rationale $m^{\text{res},t}$, in contrast to proper actions and rationale at higher SNR in Fig. 3c. Finally, Fig. 3d shows the DL message without in-context learning, i.e., $K = 0$, which fails to understand the given task, underscoring the importance of the few-shot examples c_2 in Fig. 3c and 3d.

IV. LANGUAGE-GUIDED EMERGENT COMMUNICATION

As studied in Sec. III, in-context learning enables control based on LSC without updating the LLM model, as opposed to EC necessitating MADRL training. However, LSC entails significant computing costs per inference due to the large model sizes. As shown in Table I, the floating point operations per second (FLOPs) for LSC at each UE is 890x greater than that of EC when using the BLIP [6] as $G_{\text{gen},j}(\cdot)$. Furthermore, the BS equipped with the LLaMA2-70B model [5] as $G_{\text{LLM}}(\cdot)$ incurs FLOPs that is 520 million times larger than that of EC. To mitigate this, we propose LEC that transfers the LSC’s knowledge into EC via KD as elaborated next.

A. Teacher Knowledge Construction via LSC

We construct teacher knowledge by recording the top- L outputs H^* from the set of N episodes H , generated by LSC.

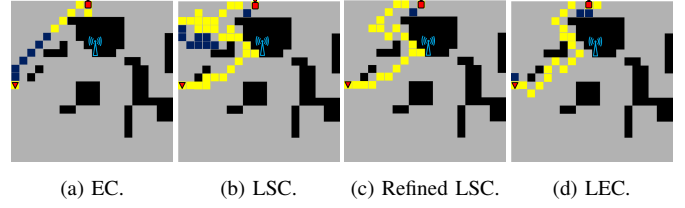


Fig. 4: Trajectory comparison among different schemes : EC, LSC, refined LSC to utilize as teacher output for LEC, and LEC.

- 1) **N -Episode Trajectory Generation via LSC:** LSC outputs H is a set defined as $H = \{H^1, H^2, \dots, H^N\}$. The n -th episode H^n consists of the records of all the UEs $\{H_1^n, H_2^n, \dots, H_{|\mathcal{J}|}^n\}$, where

$$H_j^n = \left\{ (z_j^{1,n}, a_j^{1,n}), (z_j^{2,n}, a_j^{2,n}), \dots, (z_j^{T_j^n,n}, a_j^{T_j^n,n}) \right\}. \quad (7)$$

- 2) **Invalid Action and Circular Path Removal:** Elements in H_j^n with $a_j^{t,n} = (0, 0)$ indicate invalid action, which should be removed. In addition, circular paths whereby a return to a prior location within the same episode are removed as follows. If there exist t_1 and t_2 that satisfy $t_1 < t_2$ and $z_j^{t_1,n} = z_j^{t_2,n}$, eliminate $(z_j^{t_1,n}, a_j^{t_1,n})$ pairs where $t_1 \leq t < t_2$. Retention of such ineffective pairs could misguide EC into learning wrong behaviors.
- 3) **Top- L Trajectory Selection:** L trajectories are chosen as teacher knowledge among refined H by finding n_ℓ :

$$n_\ell = \arg \min_{n \in \mathcal{N} \setminus \mathcal{N}_{\ell-1}^*} \left\{ \max_j T_j^n + \sum_{j=1}^{|\mathcal{J}|} \sum_{t=1}^{T_j} \frac{P_r}{|h_{z_j^{t,n}}|^2} \right\} \quad (8)$$

for $\ell = 1, 2, \dots, L$, where $\mathcal{N} = \{1, 2, \dots, N\}$, $\mathcal{N}_\ell^* = \{n_1, n_2, \dots, n_\ell\}$, and $\mathcal{N}_0^* = \phi$. The process finds L outputs within the minimum sum of the maximum episode length across all UEs, denoted by $\max_j T_j$, and UL power consumption $P_r/|h_{z_j^{t,n}}|^2$. Consequently, the teacher knowledge H^* is constructed as $H^* = \{H^{n_1}, H^{n_2}, \dots, H^{n_L}\}$.

B. Knowledge Distillation from LSC to EC

Based on the constructed teacher knowledge involving LSC’s top- L refined trajectories, LEC applies KD by penalizing the difference between the outputs of EC and the teacher as elaborated next.

- 1) **KLD Regularization:** A Kullback-Leibler divergence (KLD) term $\mathcal{L}_{\text{KLD}} := D_{\text{KLD}}(p(a_j^t|\theta)||p(a_j^t|H^*))$ is incorporated into the loss function when the UE’s current position z_j^t aligns with z_j^ℓ to let LEC mimic the action of H^* . The teacher knowledge H^* offers possible

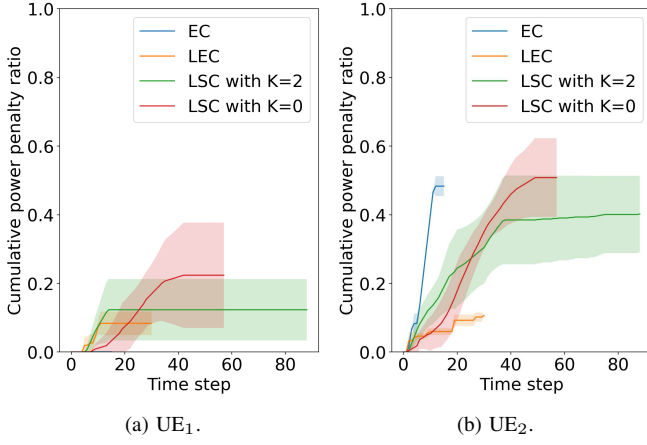


Fig. 5: Cumulative power penalty ratio (CPPR) of UE₁ and UE₂.

actions with discrete probability distribution $p(a_j^t|H^*)$ calculated as

$$p(a_j^t|H^*) = \begin{cases} \frac{\sum_{n=n_1}^{n_L} \sum_{u=1}^{T^n} \mathbf{1}_{\mathcal{B}}(u,n)}{\sum_{n=n_1}^{n_L} \sum_{u=1}^{T^n} \mathbf{1}_{\mathcal{D}}(u,n)}, & \text{if } \mathcal{D} \neq \emptyset \\ 0, & \text{otherwise.} \end{cases} \quad (9)$$

Function $\mathbf{1}_{\mathcal{D}}(u,n)$ returns 1 if $(u,n) \in \mathcal{D}$ where $\mathcal{D} := \{(u,n) | \mathbf{z}_j^t = \mathbf{z}_j^{u,n}\}$ and $\mathbf{1}_{\mathcal{B}}(u,n)$ returns 1 if $(u,n) \in \mathcal{B}$ where $\mathcal{B} := \{(u,n) | \mathbf{z}_j^t = \mathbf{z}_j^{u,n}, a_j^t = a_j^{u,n}\}$.

- 2) **KLD Divergence Mitigation:** If $\mathcal{D} = \emptyset$, the KLD diverges, motivating UEs to replicate the teacher's path by providing rewards whenever a UE's position coincides with any \mathbf{z}_j^ℓ . So, reward term of LEC \tilde{r}_j^t is defined as

$$\tilde{r}_j^t = \begin{cases} r_j^t & \text{in (2)} \\ 0.1, & \text{if } \mathbf{z}_j^t = \mathbf{z}_j^\ell. \end{cases} \quad (10)$$

Adding the new reward term promotes adherence to the paths that are well-established in the teacher's model.

In summary, LEC finds an optimal parameter set θ_{LEC}^* via solving (12), where λ is a hyperparameter that adjusts the weight of the KLD term. Minimizing the KLD guides the UEs to the aggregated action preferences of the teacher model, thereby guiding them to locations previously navigated by the teacher model, leading to a higher reward. These processes facilitate the transfer of strategic navigation knowledge from LSC to EC, thus able to determine policy via

$$(\text{LEC}) \quad a_j^t = \arg \max_a p(a|s_j^t, h_j^t, \tilde{m}_j^{\text{dn},t}; \theta_{\text{LEC}}^*), \quad (11)$$

where θ_{LEC}^* denotes the model after KD, given in (12).

V. SIMULATION RESULTS

The environment depicted in Fig. 2 and the channel coefficient at location \mathbf{z}_j^t , denoted by $h_{\mathbf{z}_j^t}$, are obtained using the ray-tracing simulator WiThRay from [14]. The environmental map has been discretized into a 20×20 grid, implying that both W_x and W_y are set to 20. The BS is located at the coordinates (6,10). For the sake of simplification, the number of UEs is limited to two, i.e., $|\mathcal{J}| = 2$, with their respective initial

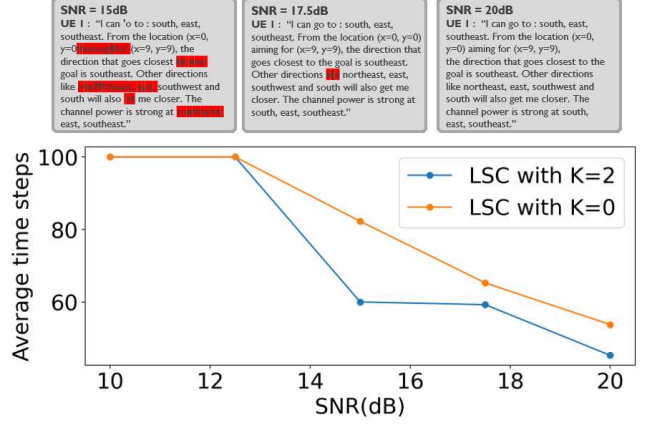


Fig. 6: Effect of in-context learning on distorted prompt.

and target positions designated as $\mathbf{z}_1^0 = (0,0)$, $\mathbf{z}_2^0 = (0,9)$, $\hat{\mathbf{z}}_1 = (9,9)$, and $\hat{\mathbf{z}}_2 = (10,0)$. The carrier frequency and the bandwidth are set as 2.3 GHz and 30.72 MHz, respectively.

Within LSC, the BLIP model is employed for the UEs. This model has been fine-tuned in advance to generate textual content enriched with action decision-relevant information. Moreover, the LLaMA2 GPTQ [15], a language model with 70 billion parameters, is integrated as $G_{\text{LLM}}(\cdot)$. Regarding EC, the following hyperparameters are a learning rate of 10^{-4} , a total of 10,000 training episodes, a discount factor γ of 1, an initial exploration probability of 0.05, an exploration probability decay ratio of 0.999, and a complex emergent message length set to 8. The experiments are conducted on NVIDIA Quadro RTX 8000 (4EA).

Multi-Modal Processing Capability and Path Uncertainty:

Fig. 4 shows UE₂ paths under EC, LSC, and LEC, with $\sqrt{\eta} = 3 \times 10^{-7}$, the global channel map illustrated as Fig. 2(c). In the grid, yellow and dark blue squares represent the UE paths, in which the locations are associated with $|h_{\mathbf{z}_j^t}|^2 \geq \eta$ and $|h_{\mathbf{z}_j^t}|^2 < \eta$, respectively. EC only takes into account navigation maps, ignoring channel maps, which results in large proportion of dark blue regions in the trajectory. Thanks to considering both location and channel maps, LSC is better at avoiding dark blue regions. However, it often yields inefficient trajectories due to the LLM's enforcing inference despite high uncertainty, i.e., hallucinations, and the resultant errors propagating through m_{t-1}^{bs} or its context window. To address this, LEC utilizes a refined trajectory in Fig. 4(c) from the original LSC's trajectory in Fig. 4(b). By selecting LSC's five trajectories out of 50 episodes, i.e., $N = 50$, $L = 5$, the MADRL training is guided using H^* with $\lambda = 1$, resulting in LEC's efficient trajectories as shown in Fig. 4(d).

Transmit Power Penalty and Travel Time: Fig. 5 examines the average cumulative power penalty ratio (CPPR) for each UE. CPPR_j^t is the ratio of the cumulative power penalty the j -th UE incurred up to a certain t when all UEs have reached their destination, calculated as $\text{CPPR}_j^t =$

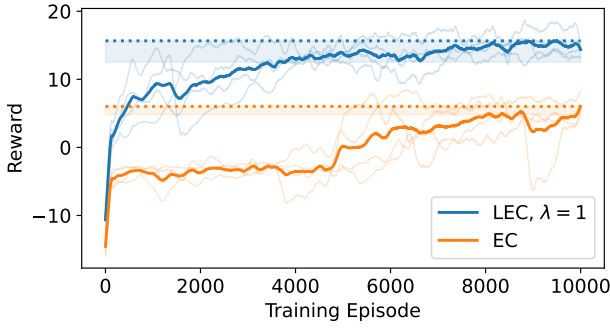


Fig. 7: Training performance and convergence of LEC and EC.

$\sum_{u=1}^t \mathbf{1}_{\mathcal{P}}(u) / \max_j(T_j)$. The function $\mathbf{1}_{\mathcal{P}}(u)$ returns 1 if $u \in \mathcal{P}$ such that $\mathcal{P} := \{w \mid |h_{\mathbf{z}_j^w}|^2 < \eta\}$, and otherwise we have 0. The solid line represents the average CPPR of the eight least time-consuming scenarios out of twenty to compare among the cases that all UEs have arrived at the destinations, while the shaded areas denote the standard deviation from the mean. In Fig. 5(a), the task for UE₁ is relatively easy thanks to its initial location and the destination, yielding low CPPRs for all schemes, only excluding LSC without in-context learning, i.e., $K = 0$. Therefore, we hereafter focus only on UE₂ depicted in Fig. 5(b). For UE₂, EC and LSC lead to high average CPPRs due to the incapability of processing multi-modal data and high path uncertainties, respectively. By contrast, LEC seeks for achieving LSC's top- L trajectories, thereby yielding fast travel time with the lowest CPPR.

Impact of In-Context Learning: Fig. 6 presents the average time steps of the two shortest and the two longest cases with LSC to reach the goal among 10 episodes with different values of SNR. We set quantized two-level global channel map as Fig. 2(d) to provide an option for UE₂ to find path with less detour. At low SNR, $\hat{m}^{\text{up},t}$ is distorted, rendering LLM unable to comprehend the input prompt and subsequently decide a proper action. This results in a random selection of actions, analogous to EC's tendency to prioritize exploration over exploitation every time step. We demonstrate the impact of few-shot learning on ambiguity reduction when input prompts are distorted by comparing scenarios with $K = 0$ and $K = 2$. The results indicate that incorporating more few-shot examples significantly reduces ambiguity and leads to fewer wrong decisions when prompts are partially distorted like demonstrated at the figure.

Convergence Acceleration via KD: Fig. 7 shows that LEC has accelerated convergence compared to EC. The thick lines are the average reward of EC and LEC along the training episodes, averaged over four different runs that are shown with transparent lines. For better visibility, the rewards are smoothed with Savitzky-Golay filter with polynomial order of 3 and window length of 301 episodes. To compare the convergence, we draw the convergence region, which is the range between the maximum reward and 80% of the maximum reward with shaded areas within the graph. LEC's average

reward curve shows fast and stable convergence by staying within the shaded convergence region from episode 3,636, whereas EC's curve fails to stay within the shaded convergence region until episode 9,520.

VI. CONCLUSION

In this paper, we explored the effectiveness of an MADRL-based EC and an LLM-based LSC in a multi-agent, multi-modal remote control and navigation task. To reap the advantages of both EC and LSC, we proposed LEC by distilling the LSC's top- L trajectory knowledge into EC, thereby achieving low computing costs at both training and inference with enhanced task performance. As a preliminary study, the current simulations rely on additive noise channels with two UEs. To enhance the feasibility of LEC, future research needs to incorporate realistic channels with more UEs. Furthermore, to cope with low SNR, DeepJSCC could be additionally utilized for the UL and DL message communication in LEC, which could be an interesting topic for future work.

REFERENCES

- [1] D. Gündüz, Z. Qin, I. E. Aguerri, H. S. Dhillon, Z. Yang, A. Yener, K. K. Wong, and C. B. Chae, "Beyond transmitting bits: Context, semantics, and task-oriented communications," *IEEE Journal on Selected Areas in Communications*, vol. 41, pp. 5 – 41, 2023.
- [2] E. Boursoulatz, D. B. Kurka, and D. Gündüz, "Deep joint source-channel coding for wireless image transmission," *IEEE Transactions on Cognitive Communications and Networking*, vol. 5, pp. 567 – 579, 2019.
- [3] J. N. Foerster, Y. M. Assael, N. D. Freitas, and S. Whiteson, "Learning to communicate with deep multi-agent reinforcement learning," *Neural Information Processing Systems*, p. 2137–2145, 2016.
- [4] S. Seo, J. Park, S.-W. Ko, J. Choi, M. Bennis, and S.-L. Kim, "Towards semantic communication protocols: A probabilistic logic perspective," *IEEE Journal on Selected Areas in Communications*, 2023.
- [5] H. Touvron *et al.*, "Llama 2: Open foundation and fine-tuned chat models," *arXiv:2307.09288*, 2023.
- [6] J. Li, D. Li, C. Xiong, and S. Hoi, "BLIP: Bootstrapping language-image pre-training for unified vision-language understanding and generation," *International Conference on Machine Learning*, p. 12888–12900, 2022.
- [7] H. Nam, J. Park, J. Choi, M. Bennis, and S. L. Kim, "Language-oriented semantic communication with semantic coding and knowledge distillation for text-to-image generation," *arXiv:2309.11127*, 2023.
- [8] J. Huang and K. C. C. Chang, "Towards reasoning in large language models: A survey," *arXiv:2212.10403*, 2022.
- [9] H. Sha *et al.*, "LanguageMPC: Large language models as decision makers for autonomous driving," *arXiv:2310.03026*, 2023.
- [10] G. Hinton, O. Vinyals, and J. Dean, "Distilling the knowledge in a neural network," *Proc. of NIPS Deep Learning Wksp., (Montreal, Canada)*, 2014.
- [11] H. Jiang, "A latent space theory for emergent abilities in large language models," *arXiv:2304.09960*, 2023.
- [12] N. Wang, J. Xie, H. Luo, Q. Cheng, J. Wu, M. Jia, and L. Li, "Efficient image captioning for edge devices," *arXiv:2212.08985*, 2022.
- [13] X. Ye. (2023) calcflops: a flops and params calculate tool for neural networks in pytorch framework. [Online]. Available: <https://github.com/MrYxJ/calculate-flops.pytorch>
- [14] H. Choi, J. Oh, J. Chung, G. C. Alexandropoulos, and J. Choi, "WiTh-Ray: A versatile ray-tracing simulator for smart wireless environments," *IEEE Access*, vol. 11, pp. 56 822–56 845, 2023.
- [15] E. Frantar, S. Ashkboos, T. Hoeffler, and D. Alistarh, "GPTQ: Accurate post-training quantization for generative pre-trained transformers," *arXiv:2210.17323*, 2022.